Inorg. Chem. **2007**, *46*, 2674–2681

Monodisperse and Core–Shell-Structured SiO_2@YBO_3:Eu^{3+} Spherical Particles: Synthesis and Characterization

Cuikun Lin, Deyan Kong, Xiaoming Liu, Huan Wang, Min Yu, and Jun Lin*

Key laboratory of Rare Earth Chemistry and Physics, Changchun Institute of Applied Chemistry, Chinese Academy of Sciences, Changchun 130022, P. R. China, and Graduate University of the Chinese Academy of Sciences, Beijing 100049, P. R. China

Received December 5, 2006

$Y_{0.9}Eu_{0.1}BO_3$ phosphor layers were deposited on monodisperse SiO_2 particles of different sizes (300, 570, 900, and 1200 nm) via a sol–gel process, resulting in the formation of core–shell-structured SiO_2@$Y_{0.9}Eu_{0.1}BO_3$ particles. X-ray diffraction (XRD), field emission scanning electron microscopy (FE-SEM), transmission electron microscopy (TEM), photoluminescence (PL), and cathodoluminescence (CL) spectra as well as lifetimes were employed to characterize the resulting composite particles. The results of XRD, FE-SEM, and TEM indicate that the 800 °C annealed sample consists of crystalline YBO_3 shells and amorphous SiO_2 cores, in spherical shape with a narrow size distribution. Under UV (240 nm) and VUV (172 nm) light or electron beam (1–6 kV) excitation, these particles show the characteristic $^5D_0$–$^7F_{1-4}$ orange-red emission lines of Eu^{3+} with a quantum yield ranging from 36% (one-layer $Y_{0.9}Eu_{0.1}BO_3$ on SiO_2) to 54% (four-layer $Y_{0.9}Eu_{0.1}BO_3$ on SiO_2). The luminescence properties (emission intensity and color coordinates) of Eu^{3+} ions in the core–shell particles can be tuned by the coating number of $Y_{0.9}Eu_{0.1}BO_3$ layers and SiO_2 core particle size to some extent, pointing out the great potential for these particles applied in displaying and lightening fields.

1. Introduction

The synthesis of nanostructured inorganic materials with hierarchical morphologies has attracted considerable attention in the fields of catalysis, separation technology, microelectronic devices, and biomaterials engineering.[1−7] In particular, the term core−shell nowadays comprises a huge area of particles that are in the broadest sense defined by a core of matter that is surrounded by a shell of different matter.[8−11] Core−shell composite materials can act as monodisperse spherical particles with good optical performance for applications. There are numerous methods of preparing core−shell structured materials, including vapor deposition, plasma-assisted techniques, chemical reduction, and self-assembly.[12] In most cases, the degree of surface coverage is low and the coating is nonuniform.[13] The sol−gel process is an effective method for preparing such materials since the reactants can be homogeneously mixed at the molecular level in solution.

On the other hand, phosphor particles with spherical morphology, nonaggregation, and the size 0.5−2 μm can improve the optical performance for field emission displays (FED) and plasma display panels (PDP) because of the high packing density and the reduction of light scattering.[14,15] Nowadays, many synthetic routes have been developed to control the size and distribution of phosphor particles, such as spray pyrolysis[16] and fluxes precipitation,[17] but the

* To whom correspondence should be addressed. E-mail: jlin@ciac.jl.cn.

(1) Radtchenko, I. L.; Sukhorukov, G. B.; Gaponik, N.; Kornowski, A.; Rogach A. L.; Mohwald, H. *Adv. Mater.* **2001**, *13*, 1684.
(2) Kresge, C. T.; Leonowicz, M. E.; Roth, W. J.; Vartuli, J. C.; Beck, J. S. *Nature* **1992**, *359*, 710.
(3) Yang, H.; Coombs, N.; Ozin, G. A. *Nature* **1997**, *386*, 692.
(4) Zhao, D.; Feng, J.; Huo, Q.; Melosh, N.; Fredrickson, G. H.; Chmelka, B. F.; Stucky, G. D. *Science* **1998**, *279*, 548.
(5) Braun, P. V.; Osenar, P.; Stupp, S. I. *Nature* **1996**, *380*, 325.
(6) Liu, J.; Shin, Y.; Nie, Z.; Chang, J. H.; Wang, L. Q.; Fryxell, G. E.; Samuels, W. D.; Exarhos, G. J. *J. Phys. Chem. A* **2000**, *104*, 8328.
(7) Guo, C. W.; Cao, Y.; Xie, S. H.; Dai, W. L.; Fan, K. N. *Chem. Commun.* **2003**, 700.
(8) Schneider, J. J. *Adv. Mater.* **2001**, *13*, 529.
(9) Zhong, C. J.; Maye, M. M. *Adv. Mater.* **2001**, *13*, 1507.
(10) Fleming, M. S.; Mandal, T. K.; Walt, D. R. *Chem. Mater.* **2001**, *13*, 2210.
(11) Yu, M.; Lin, J.; Fang, J. *Chem. Mater.* **2005**, *17*, 1783.
(12) Jiang, Z. J.; Liu, C. Y. *J. Phys. Chem. B* **2003**, *107*, 12411.
(13) Caruso, R. A.; Antonietti, M. *Chem. Mater.* **2001**, *13*, 3272.
(14) Kang, Y. C.; Lenggoro, I. W.; Park, S. B.; Okuyama, K. *Mater. Res. Bull.* **2000**, *35*, 789.
(15) Jing, X.; Ireland, T. G.; Gibbons, C.; Barber, D. J.; Silver, J.; Vecht, A.; Fern, G.; Trogwa, P.; Morton, D. *J. Electrochem. Soc.* **1999**, *146*, 4546.
(16) Cho, S. H.; Yoo, J. S.; Lee, J. D. *J. Electrochem. Soc.* **1998**, *145*, 1017.

10.1021/ic062318j CCC: $37.00
Published on Web 03/06/2007

Table 1. Experimental Conditions for the Synthesis of SiO_2 Particles with Different Sizes[a]

SiO_2 (nm)	C(TEOS)	$C(H_2O)$	$C(NH_3)$	seeds (nm)	V_{TEOS}/V_{H_2O}	N	t
300	0.17	7.5	1.0				
570	0.18	5.0	7.0				
900	0.2	5.0	7.0	500	1/2	2	3
1200	0.2	6.0	2.0	500	1/2	5	3

[a] *N*: number of reaction. *t*: reaction time (h). *C*: concentration (mol/L).

obtained phosphor particles are still far from the ideally monodisperse spherical morphology.

Silica can be easily made in spherical morphology from nanometer to micrometer size.[18] If the silica spheres are coated with layers of phosphors, a kind of core−shell-structured phosphor material with spherical morphology will be obtained, and the size for the phosphor particles can be controlled by the silica cores. Furthermore, because silica is cheaper than most of the phosphor materials (which often employ the expensive rare-earth elements as the activators and/or host components), the core−shell phosphor materials will be cheaper than the pure phosphor materials in unit mass. It is well-known that phosphors based on orthoborates have attracted much attention due to their high stability, low synthesis temperature, and high ultraviolet and optical damage threshold.[19−23] Rare-earth orthoborates have proved to be such useful host lattices for the luminescence of Eu^{3+}, which has found wide applications in Hg-free fluorescent lamps and various kinds of display devices.[24−27] Among them, YBO_3, which processes the hexagonal vaterite-type structure and shows a good vacuum ultraviolet (VUV) absorption, has been a promising host material for VUV phosphors. For example, YBO_3:Eu^{3+} is currently used as a red component in PDP television. However, conventional solid-state reaction derived YBO_3:Eu^{3+} phosphors have bad morphology (large aggregates in several micrometers) due to the high annealing temperature and repeat grinding process, which will limit its dispersing stability and subsequent coating ability on the display panels.[27b] As a result, YBO_3:Eu^{3+} phosphors with homogeneous and monodisperse spherical morphology are highly desired.

In this paper, by surface functionalization of silica particles (with size ranging from 300 to 1200 nm) with YBO_3:Eu^{3+} phosphor layers via a sol−gel process, we obtained a kind of core−shell-structured SiO_2@YBO_3:Eu^{3+} phosphor with uniform and monodisperse spherical morphology. Detailed characterizations for the structure, morphology, and luminescent properties of the samples were performed.

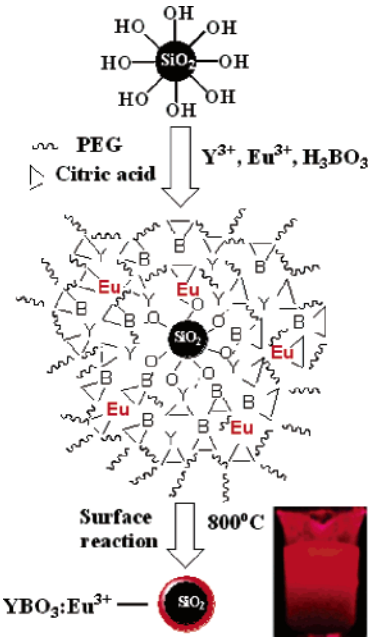

Figure 1. Formation process of SiO_2@$Y_{0.9}Eu_{0.1}BO_3$ core−shell particles with the corresponding luminescent photograph of water dispersion under 254 nm UV irradiation.

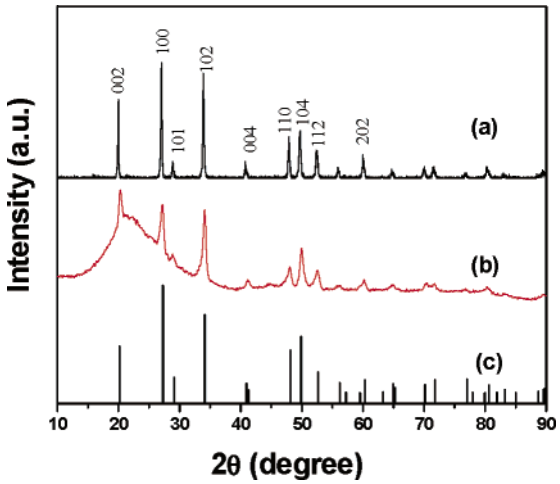

Figure 2. X-ray diffraction patterns for the 800 °C annealed pure $Y_{0.9}Eu_{0.1}BO_3$ powder (a), SiO_2@$Y_{0.9}Eu_{0.1}BO_3$ core−shell particles (b), and the JCPDS card No. 74-1929 for YBO_3 (c).

2. Experimental Section

The core−shell-structured phosphor samples with general compositions as SiO_2@$Y_{0.9}Eu_{0.1}BO_3$ were prepared by a sol−gel process. The starting materials were Y_2O_3 (99.99%, Shanghai Yuelong Nonferrous Metals Limited), Eu_2O_3 (99.99%, Shanghai Yuelong Nonferrous Metals Limited), H_3BO_3 (analytical reagent, AR, Beijing Beihua Chemicals Co., Ltd.), glycerol (AR, Beijing Beihua Chemicals Co., Ltd.), tetraethyl orthosilicate, $Si(OC_2H_5)_4$ (TEOS, 99%, AR, Beijing Beihua Chemicals Co., Ltd.), ammonium hydroxide, NH_4OH (25−28 wt %, AR, Beijing Beihua Chemicals Co., Ltd.), polyethylene glycol (PEG, molecular weight = 20000,

(17) Celikkaya, A.; Akinc, M. *J. Am. Ceram. Soc.* **1990**, *73*, 2360.
(18) (a) Stöber, W.; Fink, A.; Bohn, E. *J. Colloid Interface Sci.* **1968**, *26*, 62. (b) Hsu, W. P.; Yu, R.; Matijevic, E. *J. Colloid Interface Sci.* **1993**, *156*, 56.
(19) Ren, M.; Lin, J. H.; Dong, Y.; Yong, L. Q.; Su, M. Z.; You, L. P. *Chem. Mater.* **1999**, *11*, 1576.
(20) Wei, Z.; Sun, L.; Liao, C.; Yin, J.; Jiang, X.; Yan, C.; Lü, S. *J. Phys. Chem. B* **2002**, *106*, 10610.
(21) Bertrand-Chadeyron, G.; Mahiou, R.; El-Ghozzi, M.; Arbus, A.; Zambon, D.; Cousseins, J. C. *J. Lumin.* **1997**, *72*−*74*, 564.
(22) Lou, L.; Boyer, D.; Chadeyron, G.; Bernstein, E.; Mahiou, R.; Mugnier, J. *Opt. Mater.* **2000**, *15*, 1.
(23) Boyer, D.; Bertrand, G.; Mahiou, R. *J. Lumin.* **2003**, *104*, 229.
(24) Kim, K. N.; Jung, H. K.; Park, H. D. *J. Mater. Res.* **2002**, *17*, 907.
(25) Moine, B.; Mugnier, J.; Boyer, D.; Mahiou, R.; Schamm, S.; Zanchi, G. *J. Alloys Compd.* **2001**, *323*−*324*, 816.
(26) Bertrand-Chadeyron, G.; El-Ghozzi, M.; Boyer, D.; Mahiou, R.; Cousseins, J. C. *J. Alloys Compd.* **2001**, *317*−*318*, 183.
(27) (a) Bertrand-Chadeyron, G.; El-Ghozzi, M.; Mahiou, R.; Arbus, A.; Cousseins, J. C. *J. Solid State Chem.* **1997**, *128*, 261. (b) Boyer, D.; Bertrand-Chadeyron, G.; Mahiou, R.; Caperaa, C.; Cousseins, J. C. *J. Mater. Chem.* **1999**, *9*, 211.

Table 2. Unit Cell Parameters and Crystallite Size for Pure $Y_{0.9}Eu_{0.1}BO_3$ Powder and Those in the $SiO_2@Y_{0.9}Eu_{0.1}BO_3$ Core−Shell Particles

sample	*a* (nm)	*b* (nm)	*c* (nm)	cryst size (nm)
JCPDS 16-0277	0.3778	0.3778	0.8810	
$Y_{0.9}Eu_{0.1}BO_3$ powder	0.3782	0.3782	0.8810	58
$SiO_2@Y_{0.9}Eu_{0.1}BO_3$	0.3786	0.3786	0.8786	15

AR, Beijing Beihua Chemicals Co., Ltd.), nitric acid, HNO_3 (AR, Beijing Beihua Chemicals Co., Ltd.), ethanol, C_2H_5OH (AR, Beijing Beihua Chemicals Co., Ltd.), and deionized water.

First, monodisperse silica spheres with different sizes (300, 570, 900, and 1200 nm) were prepared by hydrolysis of tetraethyl orthosilicate (TEOS) in an alcohol medium in the presence of water and ammonia by a modified procedure of the well-known Stöber method.[18] This process yielded a colloidal solution of silica particles with a narrow size distribution in submicrometer range, and the particle size of silica depended on the relative concentration of the reactants. In a typical experiment, the mixture containing TEOS (99 wt %, analytical reagent, AR), H_2O, and NH_4OH (25 wt %, AR) was stirred at room temperature for 4 h, resulting in the formation of white silica colloidal suspension. The silica particles were centrifugally separated from the suspension and washed with ethanol four times. Monosized silica particles larger than 1 μm in diameter could not be obtained directly through the Stöber process, so seeded growth experiments were used.[18b] In the seeded growth experiments, a certain amount of monosize silica particles was seeded into the NH_3-H_2O-containing ethanol solution before the TEOS-containing ethanol was added to the reactor. The experimental procedure is similar to that of the Stöber process. The experimental conditions for obtaining the SiO_2 particles with size of 300, 570, 900, and 1200 nm are listed Table 1.

Second, coating of $YBO_3:Eu^{3+}$ phosphor layers on the SiO_2 particles to obtain the core−shell-structured $SiO_2@Y_{0.9}Eu_{0.1}BO_3$ particles was performed by the Pechini-type sol−gel process.[28] According to compositions in the above formula, stoichiometric amounts of Y_2O_3 and Eu_2O_3 were dissolved in the diluted HNO_3 under vigorous stirring. Then certain amounts of H_3BO_3 compound (50 at. % of excess) and water−ethanol (1:4 v/v) solution containing glycerol (molar ratio of H_3BO_3 to glycerol 1:2) were added to the solution, followed by the addition of PEG with a final concentration of 0.1 g/mL. The solution was stirred for 3 h to form a sol, and then the obtained silica particles were added under stirring. After being stirred for 3 h, the silica particles were separated by centrifugation at a speed of 4000 rpm. The separated particles were dried at 100 °C for 1 h immediately. Then the dried samples were annealed to 800 °C with a heating rate of 2 °C/min and held there for 2 h. The above process was repeated several times to increase the thickness of the $YBO_3:Eu^{3+}$ shells. The whole process is shown in Figure 1. The coating sol was evaporated in a similar process to produce the pure $YBO_3:Eu^{3+}$ powder sample for comparison.

The X-ray diffractions (XRD) for the powder samples were examined on a Rigaku-Dmax-IIB using Cu Kα radiation (λ = 0.154 05 nm). The morphology of the samples was inspected using field emission scanning electron microscope (FE-SEM, XL30, Philips) and a transmission electron microscope (TEM, JEOL-2010, 200 kV). The excitation and emission spectra were taken on a Hitachi F-4500 spectrofluorometer equipped with a 150 W xenon lamp, 1−6 kV electron gun (self-made electron gun, 10^{-6} Pa vacuum), and 172 nm VUV lamp (self-made) as the excitation source, respectively. Luminescence decay curves were obtained from a Lecroy Wave Runner 6100 digital oscilloscope (1 GHz) using a 250 nm laser (pulse width = 4 ns, gate = 50 ns) as the excitation source (Continuum Sunlite OPO). All the measurements were performed at room temperature (RT).

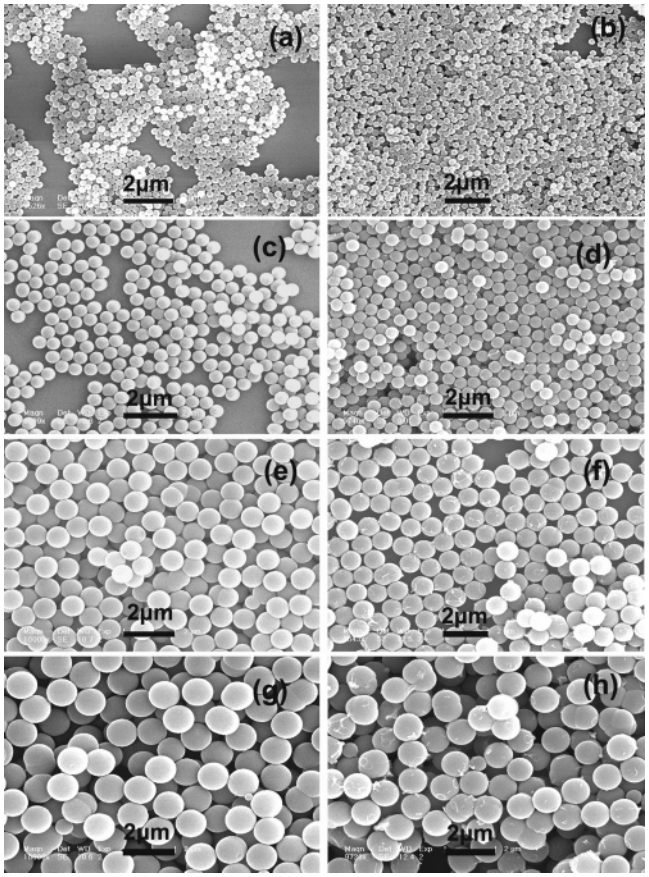

Figure 3. FESEM micrographs of the as-formed SiO_2 particles of (a) 300, (c) 570, (e) 950, and (g) 1200 nm and the (b, d, f, h) corresponding one-layer of $Y_{0.9}Eu_{0.1}BO_3$ shell coated SiO_2 particles, respectively.

3. Results and Discussion

3.1. Structure and Morphology. Figure 2 shows the XRD profiles for the 800 °C annealed pure $Y_{0.9}Eu_{0.1}BO_3$ powder (a) and core−shell-structured $SiO_2@Y_{0.9}Eu_{0.1}BO_3$ (b) samples as well as the JCPDS 16-0277 card for YBO_3 (c) as the reference, respectively. Agreeing well with the XRD peaks of pure $Y_{0.9}Eu_{0.1}BO_3$ powder, all the diffraction peaks for the core−shell-structured $SiO_2@Y_{0.9}Eu_{0.1}BO_3$ sample can be indexed according to the standard data of YBO_3 (JCPDS 16-0277), except for the broad band at $2\theta = 22^o$ from the amorphous SiO_2 (JCPDS 29-0085). No second phase was detected, indicating that no reaction occurred between the SiO_2 cores and the $Y_{0.9}Eu_{0.1}BO_3$ shells at the current annealing temperature (800 °C), and the sol−gel process is a suitable method to prepare $SiO_2@Y_{0.9}Eu_{0.1}BO_3$ core−shell particles. In general, the nanocrystallite size can be estimated from the Scherrer formula: $D_{hkl} = K\lambda/(\beta \cos \theta)$, where λ is the X-ray wavelength (0.154 05 nm), β is the full width at half-maximum, θ is the diffraction angle, K is a constant (0.89), and D_{hkl} means the size along the (*hkl*) direction.[29]

(28) (a) Yu, M.; Lin, J.; Wang, Z.; Fu, J.; Wang, S.; Zhang, H. J.; Han, Y. C. *Chem. Mater.* **2002**, *14*, 2224. (b) Yu, M.; Wang, H.; Lin, C. K.; Li, G. Z.; Lin, J. *Nanotechnology* **2006**, *17*, 3245. (c) Kong, D. Y.; Yu, M.; Lin, C. K.; Liu, X. M.; Lin, J.; Fang, J. *J. Electrochem. Soc.* **2005**, *152*, H146. (d) Pechini, M. U.S. Patent No. 3 330 697, 1967.

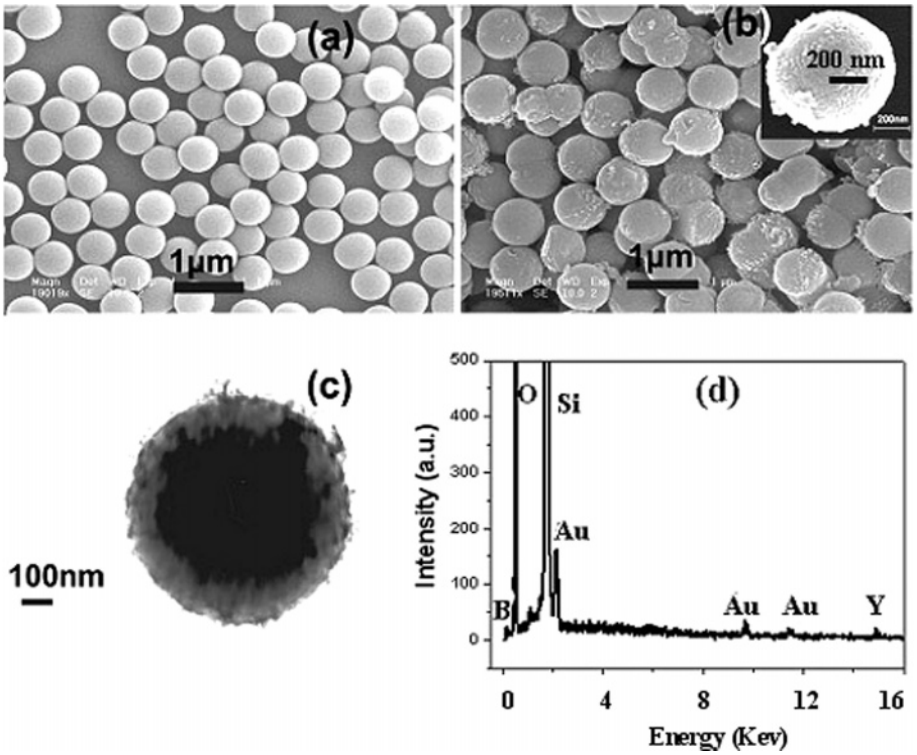

Figure 4. FESEM micrographs for as-formed SiO_2 (570 nm) (a) and four-layer of $Y_{0.9}Eu_{0.1}BO_3$ shell coated 570 nm SiO_2 particles (b) as well as the TEM micrograph (c) and EDX (d) for the particles in (b).

Table 3. Calculated Bond Lengths of $Y_{0.9}Eu_{0.1}BO_3$ in SiO_2@$Y_{0.9}Eu_{0.1}BO_3$ Core−Shell Particles

			B environment (nm)					
	Y environment (nm)		I			II		
sample	Y−O(1)	Y−O(2)	B−O(1)	B−O(2)	B−O(3)	B−O(1)	B−O(2)	B−O(3)
pure $Y_{0.9}Eu_{0.1}BO_3$	0.2321	0.2389	0.1367	0.1466	0.1573	0.1367	0.1926	0.1889
SiO_2@$Y_{0.9}Eu_{0.1}BO_3$	0.2318	0.2391	0.1366	0.1468	0.1575	0.1366	0.1923	0.1892

Here we take diffraction data along the (002), (100), (102), and (104) planes to calculate the size of the nanocrystallites, and the estimated average crystallite sizes of $Y_{0.9}Eu_{0.1}BO_3$ are around 15 nm on the SiO_2 surfaces and 58 nm for the pure $Y_{0.9}Eu_{0.1}BO_3$ powders, respectively. The XRD patterns reveal the same structure of $Y_{0.9}Eu_{0.1}BO_3$ as that of YBO_3. YBO_3 has a vaterite structure with a hexagonal $P6_3/m$ space group and cell parameters $a = 0.3776$ nm and $c = 0.8806$ nm. The yttrium atoms are 8-fold-coordinated with two nonequivalent environments. Boron atoms are 4-fold-coordinated with two types of BO_4 tetrahedra which are linked to each other giving rise to $(BO_3)^{3-}$ group.[24−27] The refined crystallographic unit cell parameters and the bond lengths were calculated for $Y_{0.9}Eu_{0.1}BO_3$ on the SiO_2 surface and pure $Y_{0.9}Eu_{0.1}BO_3$ powder, and the results are listed in Tables 2 and 3, respectively.

Figure 3 shows the SEM micrographs of the as-prepared SiO_2 particles with different sizes (a, c, e, and g) and the corresponding SiO_2@$Y_{0.9}Eu_{0.1}BO_3$ core−shell particles (b, d, f, and h), respectively. From the SEM micrographs, we can observe that the as-formed SiO_2 samples consist of spherical particles with an average size of (a) 300 nm, (c) 570 nm, (e) 950 nm, and (g) 1200 nm, and these particles are nonaggregated with narrow size distribution. After functionalizing the silica particles by one-layer of $Y_{0.9}Eu_{0.1}BO_3$ coating, the resulted SiO_2@$Y_{0.9}Eu_{0.1}BO_3$ particles are still spherical and uniform, keeping the morphological properties of the silica particles as shown in Figure 3b,d,f,g, respectively.

As a representative example, a more detailed study was performed on the silica spheres of 570 nm (Figure 4a). After being coated by four layers of $Y_{0.9}Eu_{0.1}BO_3$, the average size of these particles becomes larger (700 nm, Figure 4b), and the surface of the coated particles (inset of Figure 4b) is not as smooth as the pure ones. To investigate the detailed structure of SiO_2@$Y_{0.9}Eu_{0.1}BO_3$ core−shell samples, TEM was performed. Figure 4c shows the SiO_2 (570 nm) particles coated by four layers of $Y_{0.9}Eu_{0.1}BO_3$ layers. The core−shell structure for the SiO_2@$Y_{0.9}Eu_{0.1}BO_3$ particles can be seen clearly due to the different electron penetrability for the cores and shells. The cores are black spheres with an average size of 500 nm (a little smaller than the as-formed pure silica particles due to high temperature annealing induced condensation of the particles), and the shells have gray color with an average thickness of 100 nm. The energy-dispersive X-ray (EDX) analysis confirms the presence of B, Y, O (from the YBO_3 shells), and Si (from the silica cores), as shown

(29) Birks, L. S.; Friedman, H. *J. Appl. Phys.* **1946**, *17*, 687.

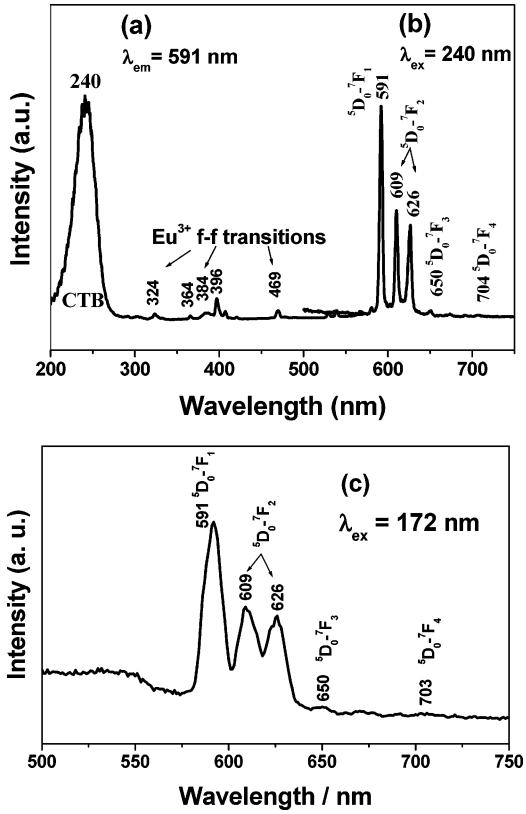

Figure 5. Excitation (a) and emission (b, c) spectra of $SiO_2@Y_{0.9}Eu_{0.1}BO_3$ core−shell sample.

in Figure 4d. The Eu element was not detected due to its low concentration (but can be detected clearly from the luminescence spectra; see next part).

Finally, we explain the formation process of the core−shell-structured phosphor particles briefly. In the Pechini sol−gel process, the citric acid first formed chelate complexes with metal ions (M^{n+}), and the left carboxylic acid groups in the citric acid reacted with polyethylene glycol to form polyester with a suitable viscosity (Figure 1). The metal ions, stabilized by the chelating and polymerizing process, were homogeneously distributed in the solution. The Stöber process-derived silica particles contained large amount of free hydroxyl groups (−OH) and silanol groups (Si−OH) on their surface.[11] When the silica particles in the solution were stirred, a lot of metal ions were absorbed onto the silica particles by physical and chemical interactions. After the drying and annealing process, the metal complexes decompose and react with each other to form the phosphor layers on the silica particles.

3.2. Luminescence Properties. 3.2.1. Photoluminescence Properties. Under the short UV (or VUV) light excitation, the $SiO_2@Y_{0.9}Eu_{0.1}BO_3$ core−shell samples exhibit a strong red emission (Figure 1). Figure 5 shows the excitation and emission spectra for $SiO_2@Y_{0.9}Eu_{0.1}BO_3$ core−shell particles. Monitored with the emission of Eu^{3+} $^5D_0-^7F_1$ transition at 591 nm, the obtained excitation spectrum (Figure 5a) consists of a broad intense band with a maximum at 240 nm as well as some weak lines between 300 and 500 nm. The strong band is due to the charge-transfer band (CTB) of $Eu^{3+}-O^{2-}$, and the weak lines arise from f−f transitions within

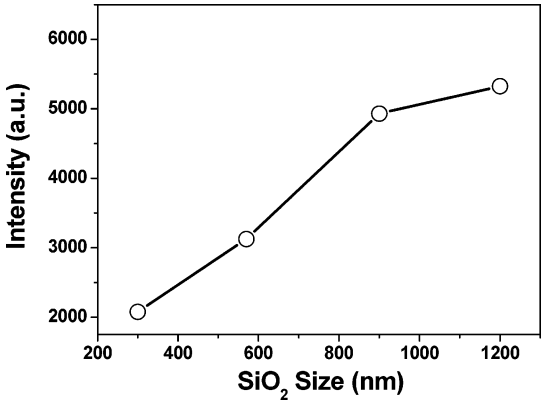

Figure 6. PL emission intensity of Eu^{3+} in $SiO_2@Y_{0.9}Eu_{0.1}BO_3$ samples as a function of the SiO_2 particle size.

the Eu^{3+} $4f^6$ electron configuration. The charge-transfer transition takes place because the Eu^{3+} ion ($4f^6$ configuration) tends to capture an electron from the O_{2p} state to achieve a more stable configuration (half-filled shell $4f^7$ configuration).[30,31] Excitation into the Eu^{3+} CTB at 240 nm yields the emission spectrum (Figure 5b) consisting of $^5D_0-^7F_J$ (J = 1−4) emission lines of Eu^{3+}, with the magnetic-dipole transition $^5D_0-^7F_1$ (591 nm) being the most prominent group.[32] A similar emission spectrum is obtained under 172 nm VUV excitation, as shown in Figure 5c.

The luminescence properties of $SiO_2@Y_{0.9}Eu_{0.1}BO_3$ core−shell phosphors can be tuned by the size of silica cores and the coating numbers (layers) of $Y_{0.9}Eu_{0.1}BO_3$. Figure 6 shows the relationship of the PL intensity of $SiO_2@Y_{0.9}Eu_{0.1}BO_3$ core−shell phosphors with the sizes of as-formed SiO_2 spheres. It can be seen clearly that the emission intensity increases with increasing the size of SiO_2 spheres. It is well-known that bigger particle size is good for the improvement of the PL intensity of phosphors.[28b] Here, it is believed that the amount of emitting Eu^{3+} ions/SiO_2 particle will increase with the increase of SiO_2 cores size, resulting in the enhancement of the PL intensity.[28b] Also, the luminescence properties of the $SiO_2@Y_{0.9}Eu_{0.1}BO_3$ core−shell samples can further be tuned by the number of $Y_{0.9}Eu_{0.1}BO_3$ layers on the SiO_2 surface. Table 4 lists a comparison for the emission properties (integrated intensity of $^5D_0-^7F_1$ and $^5D_0-^7F_2$ and their ratios *R*/*O*; total integrated intensity $^5D_0-^7F_{1-4}$, and CIE (Commission Internationale de l'Eclairage1931 chromaticity) and color coordination (x, y) for one, three, and four layers of $Y_{0.9}Eu_{0.1}BO_3$-coated SiO_2 and the pure $Y_{0.9}Eu_{0.1}BO_3$ powder samples. It can be seen that the total PL intensity of $SiO_2@Y_{0.9}Eu_{0.1}BO_3$ core−shell phosphors increases with increasing the coating number of $Y_{0.9}Eu_{0.1}BO_3$ layers, and

(30) Nakanishi, Y.; Wada, H.; Kominami, H.; Kottaisamy, M.; Aoki, T.; Hatomaka, Y. *J. Electrochem. Soc.* **1999**, *146*, 4320.
(31) Zheng, G. W.; Sun, L. D.; Liao, C. S.; Jiang, X. C.; Tao, H.; Hou, X. Y.; Jun, X. *J. Appl. Phys.* **2003**, *93*, 9783.
(32) Blasse, G.; Grabmaier, B. C. *Luminescent Materials*; Springer-Verlag: Berlin, Heidelberg, Germany, 1994; Chapter 4.
(33) (a) Zhou, Y. H.; Lin, J.; Wang, S. B. *Opt. Mater.* **2002**, *20*, 13. (b) Fouassier, C.; Saubat, B.; Hagenmuller, P. *J. Lumin.* **1981**, *23*, 408. (c) Zhang, T. R.; Spitz, C.; Antonietti, M.; Faul, C. F. J. *Chem.*—Eur. J. **2005**, *11*, 1001.
(34) Shen, W. Y.; Pang, M. L.; Lin, J.; Fang, J. *J. Electrochem. Soc.* **2005**, *152*, 25.

Table 4. Comparison of the Emission Properties (Integrated Intensity of $^5D_0-^7F_1$, $^5D_0-^7F_2$, and Their Ratios *R*/*O*; Total Integrated Intensity $^5D_0-^7F_{1-4}$, and CIE Color Coordination *x*, *y*) for One, Three, and Four Layers of $Y_{0.9}Eu_{0.1}BO_3$ Coated on SiO_2 and the Pure $Y_{0.9}Eu_{0.1}BO_3$ Powder Sample

sample	integrated intensity of $^5D_0-^7F_2$ (*R*)	integrated intensity of $^5D_0-^7F_1$ (*O*)	*R*/*O*	integrated intensity $^5D_0-^7F_{1-4}$	CIE (*x*, *y*)
SiO_2@$Y_{0.9}Eu_{0.1}BO_3$					
one-layer shell	1351.3	894.3	1.51	3126	(0.304, 0.255)
three-layer shell	3507.4	2890.4	1.21	8601	(0.435, 0.314)
four-layer shell	4284.3	3557.6	1.20	10283	(0.452, 0.318)
$Y_{0.9}Eu_{0.1}BO_3$ powder	5940.0	4984.5	1.19	13565	(0.505, 0.337)

Table 5. Integral Intensity Ratio of the $^5D_0-^7F_1$ Transition to the Total $^5D_0-^7F_j$ ($j = 1-4$) [$S_{(0-1)}/\Sigma S_{(0-j)}$] Transitions, Experimental $^5D_0$ Lifetime τ and Decay Rate k_{tot}, Calculated Radiative Rate k_r and Nonradiative Rate k_{nr}, and Absolute Quantum Yield η in SiO_2@$Y_{0.9}Eu_{0.1}BO_3$ Core−Shell Particles with One-Layer and Four-Layer $Y_{0.9}Eu_{0.1}BO_3$ Shells and in $Y_{0.9}Eu_{0.1}BO_3$ Powder Samples

sample	$S_{(0-1)}/\Sigma S_{(0-j)}$	τ (ms)	k_{tot} (ms^{-1})	k_r (ms^{-1})	k_{nr} (ms^{-1})	η (%)
SiO_2@$Y_{0.9}Eu_{0.1}BO_3$						
one-layer shell	0.349	2.52	0.397	0.143	0.254	36.0
four-layer shell	0.378	4.07	0.246	0.132	0.114	53.7
$Y_{0.9}Eu_{0.1}BO_3$ powder	0.394	3.84	0.260	0.127	0.129	48.8

the emission intensity of the four-layer $Y_{0.9}Eu_{0.1}BO_3$-coated SiO_2 sample can reach 75% that of the pure $Y_{0.9}Eu_{0.1}BO_3$ powder sample. Obviously, this can be attributed to the increase of the thickness of $Y_{0.9}Eu_{0.1}BO_3$ layers on the SiO_2 cores. Additionally, the *R*/*O* value (defined as the intensity ratio of $^5D_0-^7F_2$ to $^5D_0-^7F_1$) for one-layer $Y_{0.9}Eu_{0.1}BO_3$-coated SiO_2 sample (*R*/*O* = 1.51) is obviously larger than those for three- and four-layer $Y_{0.9}Eu_{0.1}BO_3$-coated SiO_2 samples (*R*/*O* = 1.20 for three layers and 1.21 for four layers of $Y_{0.9}Eu_{0.1}BO_3$), which are very close to that of the pure $Y_{0.9}Eu_{0.1}BO_3$ powder sample (*R*/*O* = 1.19). This can be explained as follows. First it should be stated that lower local site symmetry for Eu^{3+} will promote the $^5D_0-^7F_2$ hypersensitive transition probability (while $^5D_0-^7F_1$ remain unchanged); thus, a higher *R*/*O* value will be obtained.[20] In the core−shell-structured SiO_2@$Y_{0.9}Eu_{0.1}BO_3$ sample, the photoluminescence of Eu^{3+} contains at least two components: one comes from the (near) surface area of $Y_{0.9}Eu_{0.1}BO_3$ layers and the other from inner $Y_{0.9}Eu_{0.1}BO_3$ layers. The Eu^{3+} ions on the surface have a lower symmetrical environment, which results in a higher *R*/*O* value; while the Eu^{3+} ions in the inner $Y_{0.9}Eu_{0.1}BO_3$ layers have a higher symmetrical environment, which results in a lower *R*/*O* value. With the increase of the coating layer thickness, the ratio of the amount of Eu^{3+} ions on the surface to that of inner layers decreases. As a result, the *R*/*O* values for Eu^{3+} in three- and four-layer $Y_{0.9}Eu_{0.1}BO_3$-coated SiO_2 samples are similar to that of the pure $Y_{0.9}Eu_{0.1}BO_3$ powder sample and smaller than that in the one-layer $Y_{0.9}Eu_{0.1}BO_3$-coated SiO_2 sample (one layer, ∼10−20 nm, Supporting Information Figure S1; four layers, ∼100 nm, Figure 4c). Moreover, if the YBO_3 shell is thin enough (for example, one layer, around 10−20 nm), the Eu^{3+} ions in the interface regions (with lower local site symmetry) might be excited, resulting in a higher *R*/*O* value.

The decay curves for the luminescence of Eu^{3+} (detected at 591 nm for $^5D_0-^7F_1$ transition) in core−shell-structured SiO_2@$Y_{0.9}Eu_{0.1}BO_3$ and pure $Y_{0.9}Eu_{0.1}BO_3$ samples are shown in Figure S2 [Supporting Information, (a) for one layer and (b) for four layers of $Y_{0.9}Eu_{0.1}BO_3$ and (c) for pure $Y_{0.9}Eu_{0.1}BO_3$, respectively]. In general, all the decay curves in Figure S2 can be fitted by a single-exponential function as $I(t) = I_0 \exp(-t/\tau)$ (where I_0 is the initial intensity for $t = 0$ and τ is the lifetime), and the lifetimes of Eu^{3+} ($^5D_0$ lowest excited state) are determined to be 2.52 ms for one-layer $Y_{0.9}Eu_{0.1}BO_3$ (on SiO_2), 4.07 ms for four-layer $Y_{0.9}Eu_{0.1}BO_3$ (on SiO_2), and 3.84 ms for the pure $Y_{0.9}Eu_{0.1}BO_3$ powder sample, respectively.

Because of the invariability character for the intensity of $^5D_0-^7F_1$ transition of Eu^{3+}, it can be taken as a reference for the calculation of the luminescent quantum yield of Eu^{3+}.[35,36] On obtaining the intensity parameters of the Eu^{3+} emission spectrum, the total radiative rate of $^5D_0$ can be expressed by eq 1, where $k_{r(0-1)}$ is the radiative rate of the $^5D_0-^7F_1$ transition.[37,38] Since in vacuum, $[k_{r(0-1)}]_{vac} = 14.65$ s^{-1}, when an average index of refraction *n* equal to 1.506 was considered, the value of $k_{0-1} = n^3[k_{r(0-1)}]_{vac} \approx 50$ s^{-1} and $S_{(0-j)}$ and $S_{(0-1)}$ are the integral intensities of the $^5D_0-^7F_j$ and $^5D_0-^7F_1$ transitions, respectively:[36,37-42]

$$k_i = k_{r(0-1)} \frac{\sum_{j=0}^{4} S_{(0-j)}}{S_{(0-1)}} \quad (1)$$

The related data for Eu^{3+} in SiO_2@$Y_{0.9}Eu_{0.1}BO_3$ (one-layer, four-layer) and in the pure $Y_{0.9}Eu_{0.1}BO_3$ powder samples are listed in Table 5. From these data, the total decay rate of $^5D_0$ (K_{tot}) can be calculated according to eq 2, and the quantum yield (η) values can be estimated by eq 3. The quantum yield values seem low considering that the material

(35) Naber, R. C. G.; Blom, P. W. M.; Gelinck, G. H.; Marsman, A. W.; de Leeuw, D. M. *Adv. Mater.* **2005**, *14*, 2692.
(36) Peng, C.; Zhang, H.; Yu, J.; Meng, Q.; Fu, L.; Li, H.; Sun, L.; Guo, X. *J. Phys. Chem. B* **2005**, *109*, 15278.
(37) Yamase, T.; Kobayashi, T.; Sugeta, M.; Naruke, H. *J. Phys. Chem. A* **1997**, *101*, 5046.
(38) Carlos, L. D.; Messadeq, Y.; Brito, H. F.; Sa-Ferreira, R. A.; de Zea Bermudz, V.; Ribeiro, S. J. L. *Adv. Mater.* **2000**, *12*, 594.
(39) Sugeta, M.; Yamase, T. *Bull. Chem. Soc. Jpn.* **1993**, *66*, 444.
(40) Werts, M. H. V.; Jukes, R. T. F.; Verhoeven, J. W. Phys. *Chem. Chem. Phys.* **2002**, *4*, 1542.
(41) Hazenkamp, M. F.; Blasse, G. *Chem. Mater.* **1990**, *2*, 105.
(42) Ribeiro, S. J. L.; Dahmouche, K.; Ribeiro, C. A.; Santilli, C. V.; Pulcinelli, S. H. J. *J. Sol-Gel Sci. Technol.* **1998**, *13*, 427.

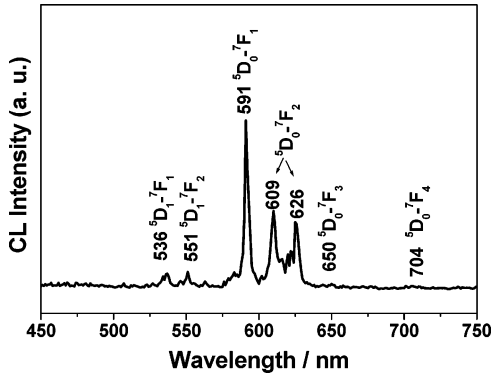

Figure 7. CL emission spectrum $SiO_2@Y_{0.9}Eu_{0.1}BO_3$ core−shell sample (accelerating voltage = 3 kV; current = 17 mA).

generally leads to high quantum yields for this rare earth ion. This may be due to the concentration quenching effect. It should be noted that eq 3 describes the quantum efficiency of the Eu^{3+} $^5D_0$ level and not the absolute emission quantum yield of the samples. The absolute emission quantum yield is a more general quantity that involves the ratio between the light absorption and the light emission. Therefore, the absolute emission quantum yield and the quantum efficiency of the $^5D_0$ level are equal, if all the energy absorbed is transferred to the $^5D_0$ level.

$$k_{\text{tot}} = \frac{1}{\tau} = k_r + k_{nr} \tag{2}$$

$$\eta = \frac{k_r}{k_r + k_{nr}} \tag{3}$$

Although the above calculation for the quantum yield is not very accurate, it tells us that the $SiO_2@Y_{0.9}Eu_{0.1}BO_3$ (four-layer) core−shell sample is comparable to the pure $Y_{0.9}Eu_{0.1}BO_3$ powder in optical performance.

3.2.2. Cathodoluminescence Properties. The cathodoluminescence (CL) of the above core−shell phosphors was also investigated. Figure 7 shows the CL spectrum of the $SiO_2@Y_{0.9}Eu_{0.1}BO_3$ core−shell sample, which is similar to the corresponding PL emission spectra in Figure 5. The CL emission intensities for four-layer $SiO_2@Y_{0.9}Eu_{0.1}BO_3$ core−shell samples have been investigated as a function of accelerating voltage and filament current, as shown in Figure 8a,b, respectively. When the filament is fixed at 14 mA, the CL intensity of the core−shell samples increases with raising the acceleration voltage from 2 to 6 kV (Figure 8a). Similarly, under 3 kV electron beam excitation, the CL intensity of the core−shell samples also increases with increasing the filament current from 14 to 18 mA (Figure 8b). For cathodoluminescence, the Eu^{3+} ions are excited by the plasma produced by the incident electrons. The electron penetration depth can be estimated by

$$L\ (\text{Å}) = 250\left(\frac{A}{\rho}\right)\left(\frac{E}{Z^{1/2}}\right)^n \tag{4}$$

where $n = 1.2/(1 - 0.29 \log_{10} Z)$, A is the atomic weight, ρ is the density, Z is the atomic number, and E is the

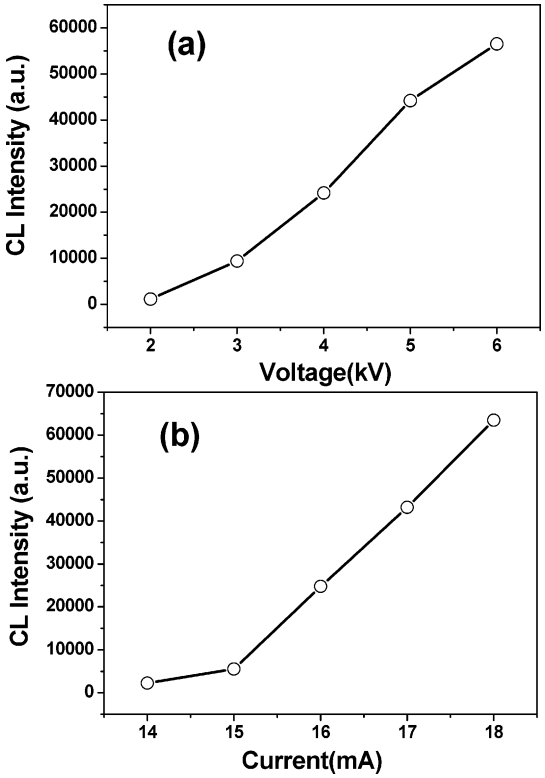

Figure 8. CL emission intensity of Eu^{3+} as a function of accelerating voltage (a) and filament current (b) in $SiO_2@Y_{0.9}Eu_{0.1}BO_3$ core−shell sample.

accelerating voltage (kV).[43−45] For $Y_{0.9}Eu_{0.1}BO_3$, the calculated electron penetration depth at 5 kV is 3.8 nm. This value is within the $Y_{0.9}Eu_{0.1}BO_3$ shell thickness for the $SiO_2@Y_{0.9}Eu_{0.1}BO_3$ core−shell particles. With the increase of accelerating voltage, more plasma will be produced by the incident electrons, resulting in more Eu^{3+} being excited and higher CL intensity. The increase in electron energy is attributed to deeper penetration of electron into the shell which is governed by eq 4. The deeper penetration of electrons in the shell results in an increase in electron−solid interaction volume in which excitation of Eu^{3+} ions is responsible for the light emission. Therefore, an increase in interaction volume (which effectively determines the generation of light inside the shell) with an increase in electron energy brings about an increase in CL brightness of $SiO_2@Y_{0.9}Eu_{0.1}BO_3$ core−shell particles.[46]

4. Conclusions

Spherical core−shell-structured $SiO_2@Y_{0.9}Eu_{0.1}BO_3$ particles with different sizes were successfully prepared by a sol−gel process followed by annealing at high temperature. Under UV light, 172 nm VUV light and 1−6 kV electron gun excitation, the Eu^{3+} ions show their characteristic orange-red ($^5D_0$−$^7F_1$) emissions in crystalline $SiO_2@Y_{0.9}Eu_{0.1}BO_3$ core−shell phosphor samples. The luminescence properties

(43) Bette, H. A. *Ann. Phys. (Leipzig)* **1930**, *5*, 325.
(44) Wang, H.; Lin, C. K.; Liu, X. M.; Lin, J.; Yu, M. *Appl. Phys. Lett.* **2005**, *87*, 181907.
(45) Feldman, C. *Phys. Rev.* **1960**, *117*, 455.
(46) Kumar, D.; Cho, K. G.; Chen, Z.; Craciun, V.; Holloway, P. H.; Singh, R. K. *Phys. Rev. B* **1999**, *60*, 13331.

of $SiO_2@Y_{0.9}Eu_{0.1}BO_3$ core−shell phosphors can be tuned by the size of silica cores and the coating numbers (layers) of $Y_{0.9}Eu_{0.1}BO_3$. The PL intensities of $SiO_2@Y_{0.9}Eu_{0.1}BO_3$ increase with increasing the coating numbers and the size of as-formed SiO_2, and the CL intensities increase with increasing the filament current and accelerating voltage. The advantages of the core−shell-structured phosphors prepared by this process include the easy availability of homogeneous spherical morphology in different size and its wide practicality for other phosphor materials, which have great potential for application in displaying and lightening fields.

Acknowledgment. This project is financially supported by the foundation of "Bairen Jihua" of the Chinese Academy of Sciences, the National Natural Science Foundation of China (Grants 50225205, 50572103, 20431030, 00610227), and the MOST of China (Grant No. 2003CB314707). M.Y. is grateful for the special starting research fund for the Awardees of President Prize of Chinese Academy of Sciences (2005−2007).

Supporting Information Available: TEM micrograph for one-layer $Y_{0.9}Eu_{0.1}BO_3$-coated SiO_2 particles (Figure S1) and decay curves for the luminescence of Eu^{3+} (Figure S2). This material is available free of charge via the Internet at http://pubs.acs.org.

IC062318J